Research Article | Vol. 26, No. 6 | 19 Mar 2018 | OPTICS EXPRESS A331
Optics EXPRESS

Comparison of metal/polymer back reflectors with half-sphere, blazed, and pyramid gratings for light trapping in III-V solar cells

TIMO AHO,[1,*] MIRCEA GUINA,[1] FARID ELSEHRAWY,[2] FEDERICA CAPPELLUTI,[2] MARIANNA RAAPPANA,[1] ANTTI TUKIAINEN,[1] A. B. M. KHAIRUL ALAM,[3] ISMO VARTIAINEN,[4] MARKKU KUITTINEN,[3] AND TAPIO NIEMI[1]

[1]*Optoelectronics Research Centre, Laboratory of Photonics, Tampere University of Technology, P.O. Box 527, FI-33101 Tampere, Finland*
[2]*Department of Electronics and Telecommunications, Politecnico di Torino, Corso Duca degli Abruzzi 24, 10129 Torino, Italy*
[3]*Institute of Photonics, University of Eastern Finland, P.O. Box 111, FI-80101 Joensuu, Finland*
[4]*Dispelix Oy, Spektri Business Park - Duo, Metsänneidonkuja 6, FI-02130 Espoo, Finland*
[*]*timo.a.aho@tut.fi*

Abstract: We report on the fabrication of diffraction gratings for application as back contact reflectors. The gratings are designed for thin-film solar cells incorporating absorbers with bandgap slightly lower than GaAs, i.e. InAs quantum dot or GaInNAs solar cells. Light trapping in the solar cells enables the increase of the absorption leading to higher short circuit current densities and higher efficiencies. We study metal/polymer back reflectors with half-sphere, blazed, and pyramid gratings, which were fabricated either by photolithography or by nanoimprint lithography. The gratings are compared in terms of the total and the specular reflectance, which determine their diffraction capabilities, i.e. the feature responsible for increasing the absorption. The pyramid grating showed the highest diffuse reflection of light compared to the half-sphere structure and the blazed grating. The diffraction efficiency measurements were in agreement with the numerical simulations. The validated model enables designing such metal/polymer back reflectors for other type of solar cells by refining the optimal dimensions of the gratings for different wavelength ranges.

OCIS codes: (040.5350) Photovoltaic; (050.1950) Diffraction gratings; (220.4000) Microstructure fabrication.

References and links

1. S. Bailey, J. McNatt, R. Raffaelle, S. Hubbard, D. Forbes, L. Fritzenmeier, and W. Maurer, "The future of space photovoltaics," in *2009 IEEE 34th Photovoltaic Specialists Conference (PVSC)*, (IEEE, 2009), pp. 001909.
2. D. B. Jackrel, S. R. Bank, H. B. Yuen, M. A. Wistey, J. S. J. Harris, Jr., A. J. Ptak, S. W. Johnston, D. J. Friedman, and S. R. Kurtz, "Dilute nitride GaInNAs and GaInNAsSb solar cells by molecular beam epitaxy," J. Appl. Phys. **101**(11), 114916 (2007).
3. M. A. Green, K. Emery, Y. Hishikawa, W. Warta, and E. D. Dunlop, "Solar cell efficiency tables (version 41)," Prog. Photovolt. Res. Appl. **21**(1), 1–11 (2013).
4. A. Tukiainen, A. Aho, G. Gori, V. Polojärvi, M. Casale, E. Greco, R. Isoaho, T. Aho, M. Raappana, R. Campesato, and M. Guina, "High-efficiency GaInP/GaAs/GaInNAs solar cells grown by combined MBE-MOCVD technique," Prog. Photovolt. Res. Appl. **24**(7), 914–919 (2016).
5. A. J. Ptak, D. J. Friedman, S. R. Kurtz, and R. C. Reedy, "Low-acceptor-concentration GaInNAs grown by molecular-beam epitaxy for high-current pin solar cell applications," J. Appl. Phys. **98**(9), 094501 (2005).
6. A. Aho, V. Polojärvi, V. Korpijärvi, J. Salmi, A. Tukiainen, P. Laukkanen, and M. Guina, "Composition dependent growth dynamics in molecular beam epitaxy of GaInNAs solar cells," Sol. Energy Mater. Sol. Cells **124**, 150–158 (2014).
7. A. Gubanov, V. Polojärvi, A. Aho, A. Tukiainen, N. V. Tkachenko, and M. Guina, "Dynamics of time-resolved photoluminescence in GaInNAs and GaNAsSb solar cells," Nanoscale Res. Lett. **9**(1), 80 (2014).
8. V. Polojärvi, A. Aho, A. Tukiainen, A. Schramm, and M. Guina, "Comparative study of defect levels in GaInNAs, GaNAsSb, and GaInNAsSb for high-efficiency solar cells," Appl. Phys. Lett. **108**(12), 122104 (2016).

#319895 https://doi.org/10.1364/OE.26.00A331
Journal © 2018 Received 16 Jan 2018; revised 1 Mar 2018; accepted 4 Mar 2018; published 13 Mar 2018

Optics EXPRESS

9. V. Polojärvi, A. Aho, A. Tukiainen, M. Raappana, T. Aho, A. Schramm, and M. Guina, "Influence of As/group-III flux ratio on defects formation and photovoltaic performance of GaInNAs solar cells," Sol. Energy Mater. Sol. Cells **149**, 213–220 (2016).
10. T. Aho, A. Aho, A. Tukiainen, V. Polojärvi, T. Salminen, M. Raappana, and M. Guina, "Enhancement of photocurrent in GaInNAs solar cells using Ag/Cu double-layer back reflector," Appl. Phys. Lett. **109**(25), 251104 (2016).
11. D. Redfield, "Multiple-pass thin-film silicon solar cell," Appl. Phys. Lett. **25**(11), 647–648 (1974).
12. F. Cappelluti, M. Gioannini, G. Ghione, and A. Khalili, "Numerical study of thin-film quantum-dot solar cells combining selective doping and light-trapping approaches," in *2016 IEEE 43rd Photovoltaic Specialists Conference (PVSC)*, (IEEE, 2016), pp. 1282–1286.
13. F. Cappelluti, D. Kim, M. van Eerden, A. P. Cédola, T. Aho, G. Bissels, F. Elsehrawy, J. Wu, H. Liu, P. Mulder, G. J. Bauhuis, J. J. Schermer, T. Niemi, and M. Guina, "Light-trapping enhanced thin-film III-V quantum dot solar cells fabricated by epitaxial lift-off," Sol. Energy Mater. Sol. Cells, in press (2018).
14. A. Luque and A. Martí, "Increasing the efficiency of ideal solar cells by photon induced transitions at intermediate levels," Phys. Rev. Lett. **78**(26), 5014–5017 (1997).
15. A. Mellor, A. Luque, I. Tobías, and A. Martí, "The feasibility of high-efficiency InAs/GaAs quantum dot intermediate band solar cells," Sol. Energy Mater. Sol. Cells **130**, 225–233 (2014).
16. F. Cappelluti, G. Ghione, M. Gioannini, G. J. Bauhuis, P. Mulder, J. J. Schermer, M. Cimino, G. Gervasio, G. Bissels, E. Katsia, T. Aho, T. Niemi, M. Guina, D. Kim, J. Wu, and H. Liu, "Novel concepts for high-efficiency lightweight space solar cells," in *E3S Web of Conferences, Vol. 16*, (ESA Publications Division, 2017), pp. 03007.
17. N. Baldock and M. Mokhtarzadeh-Dehghan, "A study of solar-powered, high-altitude unmanned aerial vehicles," Aircr. Eng. Aerosp. Technol. **78**(3), 187–193 (2006).
18. J. J. Schermer, G. J. Bauhuis, P. Mulder, E. J. Haverkamp, J. Van Deelen, A. T. J. Van Niftrik, and P. K. Larsen, "Photon confinement in high-efficiency, thin-film III–V solar cells obtained by epitaxial lift-off," Thin Solid Films **511**, 645–653 (2006).
19. S. Mokkapati and K. R. Catchpole, "Nanophotonic light trapping in solar cells," J. Appl. Phys. **112**(10), 101101 (2012).
20. E. Yablonovitch and O. Miller, "The Influence of the 4n2 Light Trapping Factor on Ultimate Solar Cell Efficiency," in *Optics for Solar Energy*, (Optical Society of America, 2010), paper SWA1.
21. F. Elsehrawy, F. Cappelluti, T. Aho, T. Niemi, V. Polojärvi, and M. Guina, " Back grating optimization for light trapping in thin-film quantum dot solar cells," in *19th Italian National Conference on Photonic Technologies* (2017), pp. 34.
22. A. Cattoni, H. Chen, J. Goffard, R. De Lépinau, B. Behaghel, C. Dupuis, N. Bardou, and S. Collin, "Multiresonant light trapping in ultra-thin GaAs and CIGS solar cells," in *Optical Nanostructures and Advanced Materials for Photovoltaics*, (Optical Society of America, 2017), paper PW3A.2.
23. U. Palanchoke, V. Jovanov, H. Kurz, P. Obermeyer, H. Stiebig, and D. Knipp, "Plasmonic effects in amorphous silicon thin film solar cells with metal back contacts," Opt. Express **20**(6), 6340–6347 (2012).
24. E. Antolín, A. Martí, C. D. Farmer, P. G. Linares, E. Hernández, A. M. Sánchez, T. Ben, S. I. Molina, C. R. Stanley, and A. Luque, "Reducing carrier escape in the InAs/GaAs quantum dot intermediate band solar cell," J. Appl. Phys. **108**(6), 064513 (2010).
25. F. Elsehrawy, T. Niemi, and F. Cappelluti, "Guided-mode resonance gratings for intermediate band quantum dot solar cells," in *Optical Nanostructures and Advanced Materials for Photovoltaics*, (Optical Society of America, 2017), paper PM3A.4.
26. A. Musu, F. Cappelluti, T. Aho, V. Polojärvi, T. Niemi, and M. Guina, "Nanostructures for light management in thin-film GaAs quantum dot solar cells," in *Light, Energy and the Environment*, (Optical Society of America, 2016), paper JW4A–45.
27. SU-8 negative epoxy resists, http://www.microchem.com/Prod-SU8_KMPR.htm, accessed December 2017.
28. OrmoComp UV inprint, http://www.microresist.de/en/product/hybrid-polymers-0, accessed January 2018.
29. E. D. Palik, *Handbook of optical constants of solids* (Academic press, 1997), pp. 492–443.
30. A. D. Rakić, A. B. Djurišic, J. M. Elazar, and M. L. Majewski, "Optical properties of metallic films for vertical-cavity optoelectronic devices," Appl. Opt. **37**(22), 5271–5283 (1998).
31. M. Peters, M. Rüdiger, D. Pelzer, H. Hauser, M. Hermle, and B. Bläsi, "Electro–optical modelling of solar cells with photonic structures," in *25th European PV Solar Energy Conference and Exhibition* (2010), pp. 87–91.

1. Introduction

Owing to their high power-to-weight ratio, radiation durability, and high efficiency, III-V solar cells are the solution of choice for space solar power applications. Multi-junction solar cells have shown efficiencies of over 30% under AM0 spectrum [1]. Further improvements are expected by employing lattice-matched $Ga_{1-x}In_xN_yAs_{1-y}$ sub-junctions grown by molecular beam epitaxy (MBE) [2–4]. The main advantage offered by GaInNAs is the ability to tailor the bandgap in the range from approximately 0.8 eV to 1.42 eV, while remaining lattice-matched to GaAs and Ge. However, at high N compositions ($y \geq 0.04$) required for bandgaps

Optics EXPRESS

below 0.9 eV, the photovoltaic properties of GaInNAs solar cells typically degrade due to relatively high p-type background doping level and short minority carrier diffusion lengths (<1 μm) [5–7]. High background doping level narrows the depletion region, which together with the short diffusion length limits the thickness of the absorption layer, resulting in lower quantum efficieny [6–9]. This can be alleviated by reducing the thickness of the absorber but then employing light trapping techniques for boosting up the carrier generation [10]. In general, when employing the light management, the physical thickness of the absorption layer can be reduced without sacrificing the current generation [11].

Another promising approach is represented by III-V quantum dot solar cells (QDSCs), where QDs will increase the short circuit current density (J_{sc}) of the GaAs solar cell [12,13]. QDSCs are promising devices both for bandgap tuning in multijunction cells and for realizing intermediate band solar cells (IBSCs) [14]. IBSCs may overcome the efficiency limit of single-gap cells through the absorption of two below-gap photons corresponding to interband and intraband optical transitions (which roughly set in the near-infrared and mid-infrared ranges) enabled by the nanostructured material. Under such conditions, increased photon harvesting is attained maintaining a high open circuit voltage. However, light absorption in the QD sheets is relatively low [15], which can again be mitigated by designs providing light trapping, as for example in the thin-film QDSC presented in Fig. 1.

Employing light trapping with substrate removal provides means for flexible, thinner, and lighter devices with high power-to-weight ratio. This approach enables fabrication of very thin solar cells, which would be beneficial e.g. for space and unmanned aerial vehicle applications [16,17].

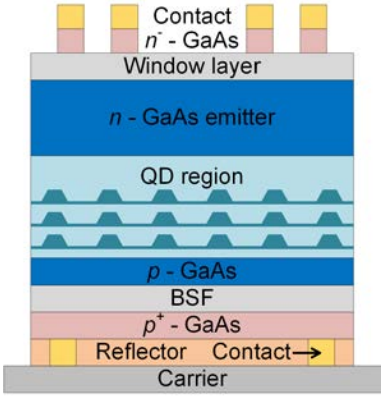

Fig. 1. Schematic structure of a thin-film QDSC employing light trapping.

As the simplest approach for improving the absorption, highly reflective planar back reflectors could effectively double the length of the optical path, increasing the J_{sc}. This approach has been demonstrated for GaAs solar cells [18], GaInNAs solar cells [10], and QDSCs [13]. The length of the optical path can be increased even more with a back reflector grating that induce light diffraction, of which various approaches have been published [19–21]. In connection with the III-V solar cells, we note for the recent work introducing nanostructures in GaAs solar cells [22].

Here, we concentrate on grating types with periods larger than the wavelength in order to have wider wavelength range in which the performance of the diffractive gratings is optimal. When the gratings are directly structured into the semiconductor, parasitic losses may occur due to surface plasmon effect resulting from the large microstructured interface area between the semiconductor and the metal [19]. However, one can use an interlayer between the semiconductor and the metal to alleviate the parasitic losses [23]. In this paper, we compare the diffraction properties of various backside gratings fabricated either by photolithography or

by nanoimprint lithography (NIL) onto a polymer. Photolithography was used as a fabrication method for photoresists and NIL was used for NIL photoresist deposited on GaAs. To study the diffraction properties of the gratings, semi-insulating GaAs (SI-GaAs) was used as a substrate, since it is almost transparent for wavelengths above 900 nm. Thus, the comparison of the gratings using reflectance measurements is possible. The gratings were optimized for light trapping at the wavelengths corresponding to the energies slightly below the bandgap of GaAs. In particular, the gratings are designed for enhancing interband transitions of typical InAs/GaAs QDSCs in the wavelength range of 900 nm – 1200 nm [13,24]. While this is sufficient for optimizing QDSCs working in the single-gap limit [13], the ideas presented in this work should be further developed to devise suitable strategies for the simultaneous enhancement of QD intersubband transitions, involving longer wavelengths [15,25].

2. Design and experiments

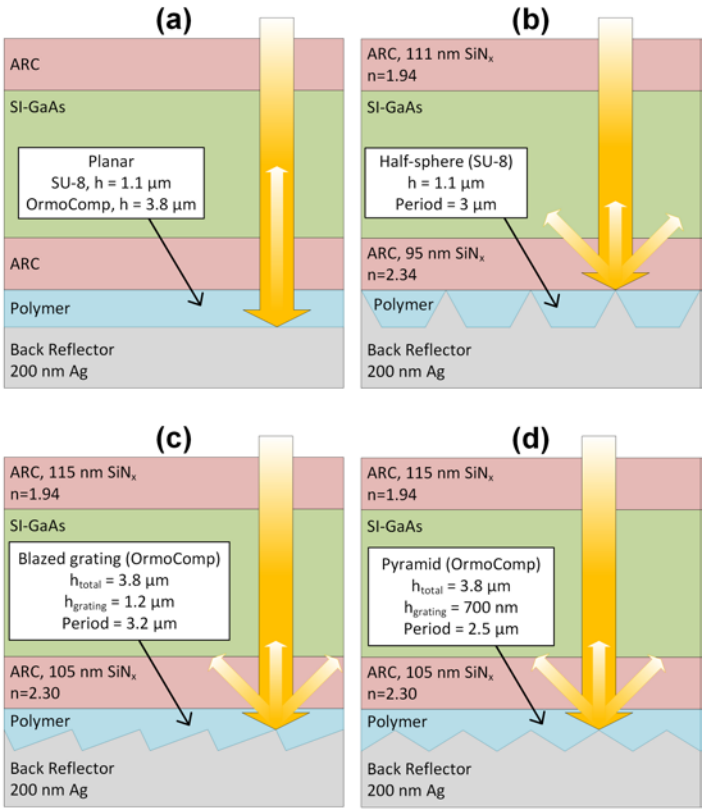

Fig. 2. The schematic drawing of the structures. (a) The planar reflector with SU-8 or OrmoComp layer, (b) the reflector with the half-sphere grating, (c) the reflector with the blazed grating, and (d) the reflector with the pyramid grating.

In this study, different structures were simulated and fabricated for assessing diffraction efficiencies and their dependence on the design features. Musu et al. [26] and Elsehrawy et al. [21] have simulated the gratings for the back reflector structures to find the optimum dimensions for absorption near the GaAs absorption edge. According to these simulations, the maximum photocurrent is achieved when the height/period aspect ratio is 0.32-0.38, which was employed to fabricate the gratings in this work. As substrate, we used double-sided polished SI-GaAs with a thickness of 350 µm. Single-layer SiN_x antireflection coatings (ARCs) were deposited by plasma enhanced chemical vapor deposition on both sides of the substrate. The front ARC was optimized to minimize the reflectance at the air/GaAs interface,

Optics EXPRESS

while the backside ARC was optimized to minimize the reflectance at the GaAs/polymer interface. The properties of the SiN_x layers were tuned by varying the process parameters such as NH_3 and SiH_4 gas flows and deposition time. The ARC thicknesses and refractive indices are presented in Fig. 2, which also introduces the three structures and the planar references.

2.1 Half-sphere grating

In the first approach, the photonic grating was fabricated by photolithography using a commercial epoxy based negative photoresist, SU-8 (MicroChem Corp.), which is commonly used in the electronic industry. SU-8 is chemically and mechanically stable and has low absorbance at least in the wavelength range from 400 nm to 1600 nm [27]. A sample with the planar SU-8 layer, shown in Fig. 2(a), was used as reference. A photolithography mask with the square openings of size 2 × 2 μm^2 and with 3 µm periodicity was used to obtain the desired half-sphere structure by varying photolithography process parameters, such as spin coating speed, exposure time, and baking temperatures. The fabricated half-spheres have height of 1.1 µm and period of 3 µm. The schematic drawing of the half-sphere grating is presented in Fig. 2(b). To realize the reflector, 200 nm Ag was deposited using electron beam evaporation on top of the polymer layer.

2.2 Blazed grating and pyramid grating

In the second and the third approach, a commercial OrmoComp NIL photoresist (Micro Resist Technology GmbH) [28] was used for two different microstructures: blazed grating in Fig. 2(c), and pyramid grating in Fig. 2(d). A commercial master (Thorlabs) and an in-house fabricated Si master were used for the blazed grating and the pyramid grating, respectively. The Si master was fabricated in two steps. First, the structure was patterned with electron beam lithography and transferred into Si by anisotropic wet etching. With this, pyramids were obtained, but the height and the aspect ratio of the pyramids were not appropriate. In order to achieve the required dimensions, the pattern was imprinted onto NIL photoresist and dry etched with desired selectivity into another Si wafer, leading to the final master. In the NIL processes, the gratings from the masters were transferred into polydimethylsiloxane stamps, which were used for imprinting the gratings into the NIL photoresist. The fabricated blazed grating has height of 1.2 µm and period of 3.2 µm and the pyramid grating has height of 700 nm and period of 2.5 µm. On top of the polymer layer, 200 nm Ag was deposited using electron beam evaporation.

2.3 Characterization of the gratings

The gratings were characterized with a Wyko NT1100 optical profilometer (Veeco Instruments Inc.) and with a scanning electron microscope (SEM) (Ultra-55, Carl Zeiss). The specular reflectance at 8° incident angle was measured with a PerkinElmer Lambda 1050 spectrophotometer. In addition, the total reflectance was measured with the integrating sphere module of the spectrophotometer. The diffuse reflectance can be retrieved by comparing the specular reflectance and the total reflectance. All the measurements were conducted through the SI-GaAs wafer and the performance of the back reflectors were evaluated at the wavelengths for which SI-GaAs is transparent.

To quantify the amount of diffracted light, the spectral diffraction efficiency was measured at diffraction orders of m = 0, ± 1, and ± 2. This measurement was carried out by variable angle measurement technique where the sample is illuminated by a white light beam at an incident angle of 8°. Diffracted light is collected at variable angles from 8° to 48° with an optical fiber connected to a spectrometer. As a result, the diffraction efficiency is defined as the diffracted power divided by the incident power. With our system, only the diffraction orders within the escape cone of the SI-GaAs wafer can be measured.

Optics EXPRESS

2.4 Simulations

The grating structures were simulated using the rigorous coupled-wave analysis method (RCWA) with the RSoft DiffractMOD software (Synopsys) and the planar structures were analyzed with transfer-matrix method. The gratings exhibit both 2D (linear gratings) and 3D (crossed gratings) configurations. In the 2D simulations, the results are an average of the TE and TM polarizations for each of the diffraction orders. In the 3D case, the gratings are symmetric and therefore both polarizations are equal for the direct angle of incidence.

The simulated gratings have the nominal geometrical features, i.e. flattening and rounding of the grating shape due to processing imperfections were not taken into account in the simulations. Numerically, the grating structure is approximated by a layered geometry with a spatial resolution of 70-75 nm. All the presented simulations use 10 harmonics for each in-plane direction. The optical model for GaAs is obtained from [29] and for Ag from [30], while constant real refractive indices are used for the ARC layers (see values in Fig. 2) and the polymers (n = 1.51).

One limitation of the RCWA method lies in the simulation of structures thicker than the coherence length of sunlight (~1 μm), because fictitious interference effects cause high-frequency noise [31]. Such artifacts can be eliminated by using e.g. the methodology presented in [31]. In this work, the results were obtained by varying the substrate thickness of ± 5 μm in 5 steps and averaging across the simulations. Further reduction of interference effects was then achieved by averaging the calculated reflectance spectra and diffraction efficiency over 10 nm wavelength interval.

3. Results and discussion

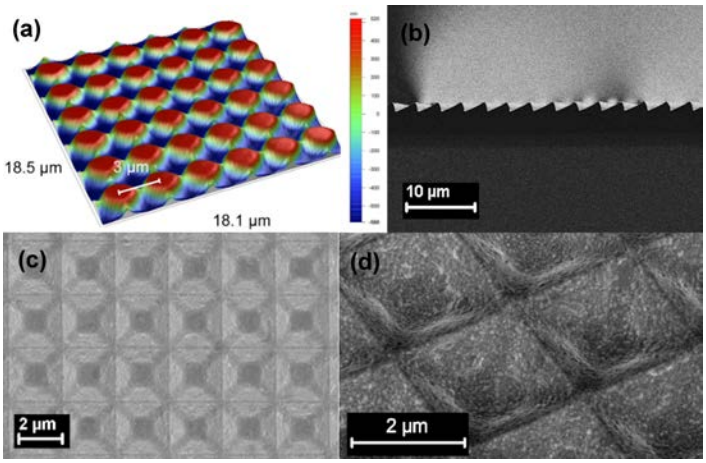

Fig. 3. (a) Optical profilometer image of the half-sphere structure, (b) Cross-sectional SEM image of the blazed grating, (c) and (d) SEM images of the pyramid grating.

Figure 3 shows the structural details of the three experimental structures: half-sphere, blazed grating, and pyramid grating. The top of the half-sphere appeared slightly flattened, as shown in the optical profilometer measurement in Fig. 3(a). The SEM images of the pyramid grating, presented in Fig. 3(c) and 3(d), are taken from the back surface of the sample where 200 nm Ag is evaporated, whereas the blazed grating image in Fig. 3(b) is the cross-section of the polymer without Ag. The pyramid grating shows flattened peak. This was already observed in the Si master, which means that the transfer of the pattern was successful and the flattening is due to the Si master.

Optics EXPRESS

3.1 Half-sphere grating results

The reflectance measurement results of the half-sphere grating are presented in Fig. 4, where the difference between the total and the specular reflectance represents the diffuse reflectance. A strong interband absorption of light into SI-GaAs is observed in the wavelengths below 900 nm, as expected. The half-sphere grating shows high diffuse reflectance, which is desired for diffraction gratings. However, a local maximum in the specular reflectance is observed, decreasing the diffuse reflectance at the target wavelength range of 950nm-1150 nm. The planar structures used as reference showed high specular reflectance and ~10% higher total reflectance. This difference is possibly originating from the diffuse reflectance, which may occur also at planar surfaces due to scattering.

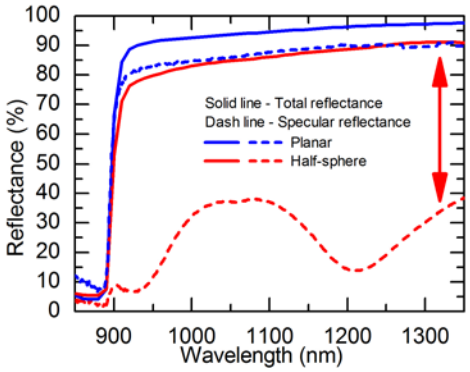

Fig. 4. Total and specular reflectance of the half-sphere structure and the planar reference. The red double-headed arrow represents the diffuse reflectance.

Figure 5 shows the measured and the 2D simulated diffraction efficiency of the half-sphere structure. The results show good correlation between measurements and simulations. Significant power coupling to the first two diffraction orders is observed. In addition, the measured diffraction efficiency of the zero order is in agreement with the specular reflectance measurements presented in Fig. 4.

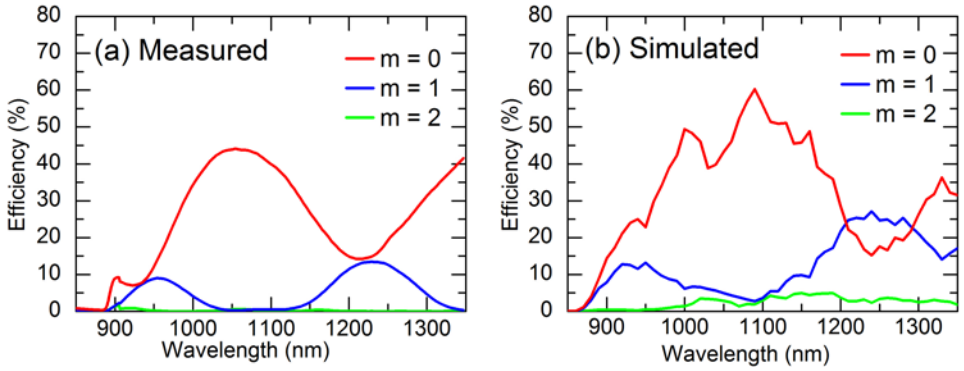

Fig. 5. The measured (a) and the simulated (b) diffraction efficiency of the half-sphere structured sample.

3.2 Blazed grating and pyramid structure results

The reflectance measurements of the blazed grating and the pyramid grating are compared in Fig. 6(a). According to the measurements, the pyramid grating shows the highest diffuse reflectance when compared to the blazed grating or the half-sphere structure. Also, the blazed grating showed low specular reflectance, which is beneficial for high diffraction of light.

Optics EXPRESS

However, the total reflectance of the blazed grating was reduced compared to the pyramid grating. This means that there are some extra losses in the structure, potentially originating from the surface plasmon resonance (SPR) in the metal reflector. This behavior can be seen also in the simulations in Fig. 6(b). The simulated total reflectance for both the blazed grating and the pyramid grating is approximately 10 percentage points lower than the measured total reflectance, since simulations are probably overestimating the losses in the structured metallic reflector. In fact, the analysis of the calculated distribution of absorbed photon density (not shown here) pointed out large optical loss at the polymer/metal interface of the patterned structures, whereas marginal optical loss was observed in the reflector of the planar structure. The lower loss observed in the experiments could be attributed to a reduction of the SPR effect owing to the flattening of the fabricated structures with respect to the nominal ones. Moreover, some inaccuracy might originate also from the simple optical model adopted for the SiN_x and polymer layers. Despite this, an overall good agreement between the measured and the simulated trends is achieved, supporting the conclusions of the diffractive properties of the structures.

As a final remark, for the planar reflector, the simulated total reflectance curve is flat, whereas the measured one is increasing towards higher wavelengths. This difference mostly arises from the residual absorption into SI-GaAs. From transmittance measurements across the SI-GaAs wafer, an extinction coefficient $k \sim 6 \times 10^{-6}$ was estimated, whereas the adopted GaAs optical model [29] uses $k = 1 \times 10^{-6}$ above 890 nm.

To display the limits imposed by the layer structure and the ARC, the front surface reflectance was simulated and is presented in Fig. 6(b). The single-layer ARC on top of the samples was designed to have the lowest reflectance at the wavelength of 900 nm. This means that part of light is reflected already from the surface of the sample without reaching the diffraction grating, increasing the measured specular reflectance.

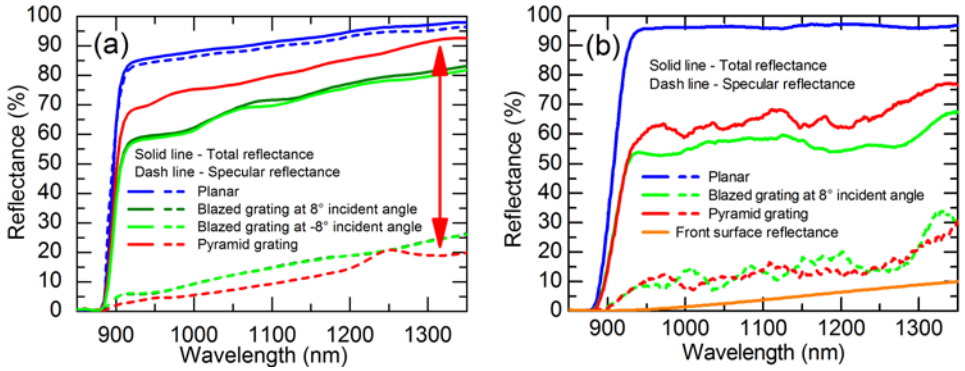

Fig. 6. The measured (a) and the simulated (b) reflectance of the blazed grating, the pyramid grating, and the planar reference. The difference between the total and the specular reflectance represents the amount of diffracted light (the red double-headed arrow).

The diffraction efficiency results of the blazed grating are presented in Fig. 7. Since the grating is asymmetric, the diffraction orders are not symmetric along the xz-plane, which is well observed at m = ± 1 and m = ± 2 diffraction orders. In addition, at m = 0, a small difference between the 8° and –8° angles of incident light is observed, due to the asymmetric grating. This difference seems to be negligible in the corresponding specular reflectance measurement shown Fig. 6(a), possibly due to the accuracy of the measurement. The diffraction orders of m = 0, + 1, and + 2 in the 2D simulations shown in Fig. 7(b) are supporting the measurements, even though they are not perfectly matching. In particular, simulations predict low frequency oscillations of the m = 0 spectrum, which were not observed in the experiments. Such oscillations could be attributed to the onset of a Fabry-Perot cavity effect in the polymer layer. The wavelength period (about 75-80 nm at λ = 1050

Optics EXPRESS

nm) is in fact well correlated with the polymer thickness and the oscillations were mainly visible in the TE polarization, which suffers less for the optical loss at the polymer/metal interface. On the other hand, such interference effects are not visible in the experimental data due to the non-uniformity of the fabricated polymer layer.

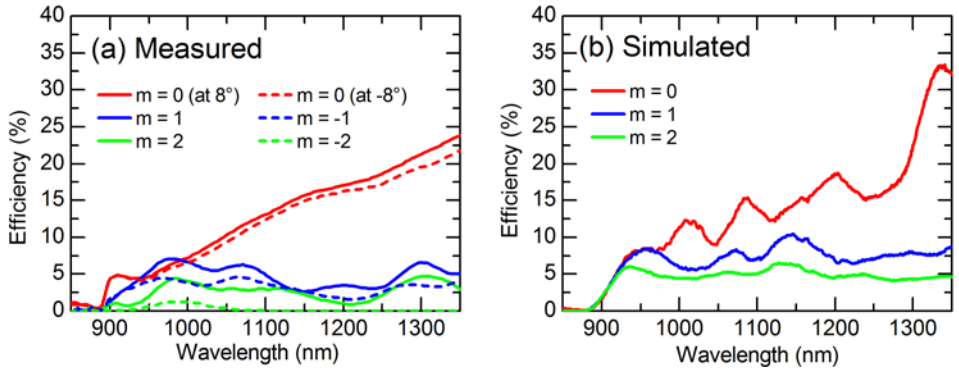

Fig. 7. The measured (a) and the simulated (b) diffraction efficiency of the blazed grating. The measurements are presented in two different directions whereas the simulations are only in single direction.

The diffraction efficiency results for the pyramid grating are presented in Fig. 8. In the measurements, power coupling to the first diffraction order is observed. The second diffraction order was not observed in the measurements, since they were performed up to 48° angle, where m = 2 is not yet present. However, according to the simulations, there is power coupling also to the second diffraction order. Furthermore, the m = 0 diffraction order is well in line with the specular reflectance results, presented in Fig. 6(a).

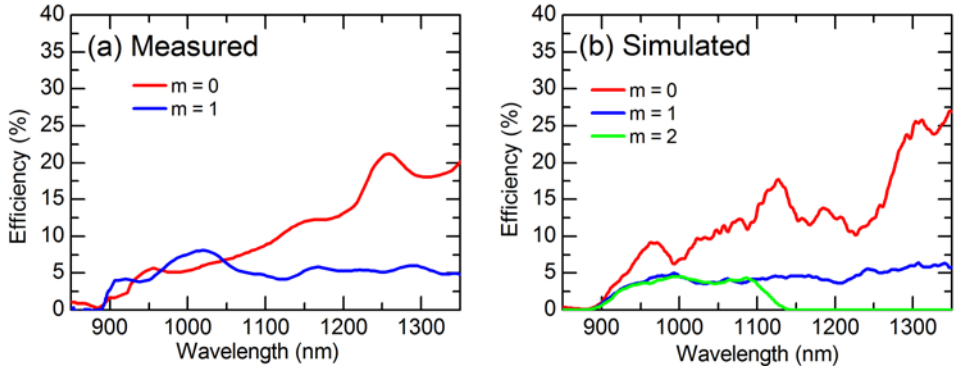

Fig. 8. The measured (a) and the simulated (b) diffraction efficiency of the pyramid grating. The measured diffraction efficiency is an average of the two directions.

3.3 Thin-film QD solar cell simulations

Implementing the studied metal/polymer back reflectors in a thin-film QD solar cell can provide significant enhancement of the QD photogenerated current. As an example we can consider a QDSC structure with 2.6 µm thick GaAs active region embedding a stack of 20 InAs/GaAs QD layers with overall thickness of about 400 nm [21,26]. The structure includes top and bottom ARC layers similar to those reported in Fig. 2. Further details on the structure can be found in [21]. The QD stack's optical model was extracted from the external quantum efficiency measurements in [13]. Figure 9 shows the calculated absorbance spectrum for the QDSC in the substrate-based configuration and for two thin-film configurations, one with planar backside reflector and one integrating the pyramid backside grating described in Sec.

3.2. The grating has period of 3 µm and height of 0.75 µm and is terminated by a 200 nm thick Ag mirror. The absorbance spectrum is calculated by integrating the absorbed photon density only in the cell active region (i.e. low-doped GaAs and QD stack), and thus is not affected by optical loss in the contact and metal layers. The pyramid grating shows a significant increase of absorbance in the QD wavelength region with respect to the reference structures. The corresponding QD photocurrent density is calculated by integrating the absorbance over the AM1.5G sun spectrum in the 895 nm – 1200 nm range. The photocurrent per QD layer turns to be about 0.024 mA/cm^2, 0.038 mA/cm^2, and 0.095 mA/cm^2 for the substrate-based, thin-film with planar reflector and polymer/metal backside grating configurations, respectively. Therefore, the light trapping scheme allows for a four times increase of the current density from the quantum dot stack. This is a remarkable result if one considers the technological effort in terms of the epitaxial growth needed to increase by a factor of four the number of QD layers or the QD areal density. As reported in [13,26], further optimization of the structure and e.g. the use of higher index materials for the grating could yield even higher current enhancement.

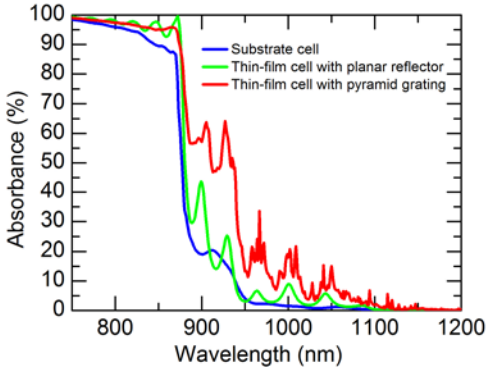

Fig. 9. Absorbance spectrum for QDSCs in three different configuration.

4. Conclusions

We studied structured metal/polymer back reflectors for the III-V solar cells with the half-sphere gratings, the blazed grating, and the pyramid grating. Efficient diffraction of light was observed for all the structures, indicating potential for improving the absorption and hence the current generation in thin-film solar cells. The pyramid grating showed the highest diffuse reflectance in the wavelengths corresponding to the photogeneration in GaInNAs solar cells and InAs/GaAs QDSCs. The microstructures can be applied to other types of solar cells by tuning the dimensions of the polymer structure to match the required wavelength range.

Funding

European Union Horizon 2020 project TFQD (Grant Agreement No. 687253); ERC AdG project AMETIST (Grant Agreement No. ERC-2015-AdG 695116); Jenny and Antti Wihuri Foundation.

Acknowledgments

Portions of this work were presented at the Light, Energy and the Environment Congress in 2017, paper JW5A.23. The author wish to thank Ville Polojärvi, Jussi-Pekka Penttinen, and Lauri Hytönen for their technical support.